Journal of Computational Chemistry

WILEY

Journal of COMPUTATIONAL CHEMISTRY

RESEARCH ARTICLE OPEN ACCESS

Revisiting the "Cluster-In-Solvent" Approach for Computational Spectroscopy: The Vibrational Circular Dichroism as a Test Case

Srilatha Arra | Isabella Daidone | Massimiliano Aschi

Department of Physical and Chemical Sciences, University of L'Aquila, L'Aquila, Italy

Correspondence: Massimiliano Aschi (massimiliano.aschi@univaq.it)

Received: 8 November 2024 | **Revised:** 12 May 2025 | **Accepted:** 20 May 2025

Funding: This work was supported by the Ministero dell'Università e della Ricerca (Grant ID: 10.13039/501100021856).

Keywords: cluster analysis | computational spectroscopy | essential dynamics | molecular dynamics | vibrational circular dichroism

ABSTRACT

The cluster-in-solvent approach, that is, the use of the quantum-mechanical calculation of a spectral observable on a significant number of solute–solvent clusters extracted from semi-classical simulations, is widely used in computational spectroscopy. However, identifying relevant coordinates for cluster selection remains a challenge. We previously developed the Ellipsoid Method for Cluster-in-Solvent (EMCS), an automated strategy for unbiased identification and statistical weighting of clusters. Yet, for larger solutes, EMCS can yield overly large solvent clusters that hinder conformational analysis. Here, we introduce a simple extension of EMCS that reduces cluster size, enabling its application to medium-to-large solutes. The method is validated through the computation of Vibrational Circular Dichroism (VCD) spectra, which are highly sensitive to solute–solvent interactions. Test cases include aqueous L-alanine, aqueous dialanine, and (1S,2S)-trans-1-amino-2-indanol in DMSO. For L-alanine and trans-1-amino-2-indanol, computed spectra closely match experiment, with root-mean-square-deviation (RMSD) values of 10.3 and 8.0, respectively, consistent with previous benchmarks. For aqueous dialanine, the main spectral features were reproduced, though discrepancies in the fine structure remain, likely due to limitations in capturing subtle solvation effects. Overall, the refined EMCS protocol enables efficient and non-arbitrary sampling of solute–solvent clusters, offering a valuable tool for the structural analysis of solvation shells in complex molecular systems.

1 | Introduction

Among the various methods proposed in the context of Soft-Matter Computational Spectroscopy [1–7] the "cluster-in-solvent" approach has proven to be one of the most extensively used. In this computational scheme [8–11] the spectral observables are calculated through quantum-chemical calculations on a series of solute–solvent clusters of limited size, extracted from semi-classical Molecular Dynamics (MD) or Monte Carlo (MC) simulations. One critical point of this protocol, beyond the obvious issue concerning the quality of the force field, is the criterion followed to choose the solute–solvent cluster internal coordinates necessary for univocally identifying the corresponding conformations. One possible strategy is based on the *brute-force* approach in which a huge number of uncorrelated solute–solvent clusters is selected from the MD or MC simulation [12, 13]. Alternatively, the conformational analysis can be addressed following, when possible, a reduced number of internal coordinates [14, 15] or even adopting more unbiased algorithms recently proposed [16]. In this respect, our group has developed [17] and applied [18, 19] a methodology (hereafter briefly termed the Ellipsoid-Method-for-Clusters-in-Solvent, EMCS) which, starting from an MD simulation of the chromophore of interest (hereafter *S*) embedded in *N* solvent

molecules (*SOLV*) allows us to unambiguously identify, and then extract, a subtrajectory of a number $M < N$ of *SOLV* contained within an ellipsoid best fitting the solute *S*. Making use of the specific features described in detail in the original paper [17] the conformational analysis of such $S(SOLV)_M$ cluster *in principle* coincides with the conformational analysis of whatever molecular system along an MD simulation. It follows that the identification of the relevant (transient) $S(SOLV)_M$ conformations, as well as their relative stability (statistical weight), can be carried out through whatever well-assessed cluster-analysis protocols normally used for analyzing molecular conformational transitions along MD trajectories [20, 21]. For this purpose, in all the EMCS applications, we have so far systematically adopted Essential Dynamics (ED) [22, 23]. The advantage of ED analysis [23] lies in its ability to identify a reduced number, typically not exceeding two or three, of generalized internal degrees of freedom (the Essential Eigenvectors, EEs), allowing a relatively straightforward conformational analysis even in complex molecular structures. However, when the number of EEs turns out to be larger than three, the conformational analysis could become very problematic from a practical point of view. This might indeed occur when ED is applied in conjunction with EMCS. In these cases, in fact, the number of EEs can rapidly become prohibitively large as the strength of the solute–solvent interaction decreases and/or the number of solvent molecules increases [18, 19].

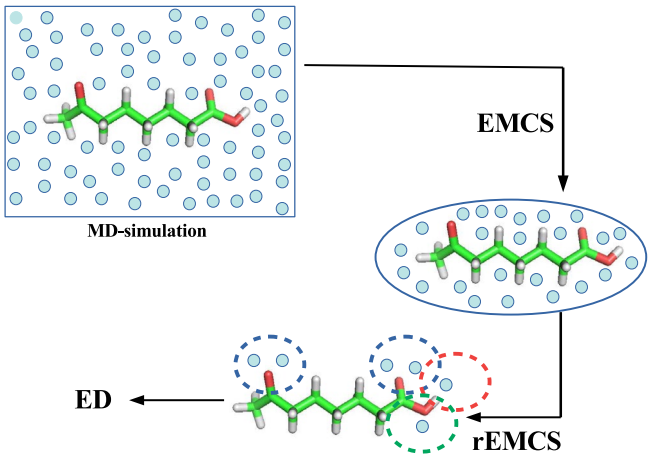

FIGURE 1 | Schematic representation of the sequential steps for rEMCS. See also the Results section. (i) The EMCS, performed on the MD-simulation, produces a subtrajectory of the solvent molecules (schematically shown as light-blue spheres) contained in the ellipsoid best approximating the solute molecule. (ii) A number of the solute atoms, conceivably capable of undergoing tighter interactions (if any) with the solvent molecules, are selected and highlighted with dotted circles. (iii) The solvent molecules falling in these selected regions are taken into account; all the other solvent molecules are removed. (iv) The reduced trajectory is analyzed through ED.

To overcome this possible drawback, we report in this study a simple method to reduce the solvent molecules in the $S(SOLV)_M$ extracted through EMCS. Our idea is inspired by the intuitive consideration that, if present, relatively stable solute–solvent microclusters can only be identified where relatively stable physical solute–solvent interactions can be formed, that is, typically at the solute–solvent interface, also termed as *first solvation shell*. Consequently, the proposed method, hereafter simply termed as reduced-EMCS (rEMCS) and schematically depicted in Figure 1, simply consists in eliminating at each frame of the $S(SOLV)_M$ cluster trajectory obtained from EMCS, all the solvent molecules not directly linked to specific parts of the *S* capable of forming more stable interactions (e.g., polar groups, Lewis acids or bases). This approach, while maintaining the features of EMCS, should allow a simplification of the subsequent ED analysis. To test its validity, we decided in the present study to apply this method to the modeling of Vibrational Circular Dichroism (VCD) spectra on a number of well-studied systems.

VCD [24–29] has become, in the last few decades, one of the most powerful tools for determining the absolute configuration of several classes of molecules [30–35]. A strong impetus to the development of this experimental technique has also been given, in the last years, by the availability of efficient theoretical-computational models [36–38] nowadays brought to extremely advanced levels of accuracy [39–53]. VCD spectral signals in condensed phase are known to depend on the explicit interaction with the solvent [53–58] as witnessed by several studies, either using the "cluster-in-solvent" approach [58–67] or using purely classical methods, based on MD simulations, exploiting the time-correlation formalism [68–73]. Because of this peculiarity, the modeling of VCD spectra appeared as particularly suitable for the main purpose of the present study: To propose a method that allows capturing the morphological characteristics of the solvation shells in a rigorous but, at the same time, simple, effective, and computationally inexpensive way. In this study we selected three well investigated systems: (i) aqueous alanine (ALA) [12], (ii) (1S,2S)-trans-1-amino-2-indanol (trans-AI) in dimethyl sulfoxide [62], and (iii) aqueous capped alanine dipeptide (ADP), Ac-Ala-NHMe [70, 74] where the crucial role of the first solvation shell, for the correct VCD modeling, has been widely discussed in the referenced studies. We wish to underline that the success of EMCS and rEMCS strongly depends on the quality of the MD simulations (both force field and length of the trajectory) and on the level of the quantum-chemical calculation for the spectral observable. All these aspects have not been addressed in this study, whose primary aim was to describe the proposed approach using model systems already addressed by other groups. This study is organized as follows. In the first section (Computational details), after a brief outline of the general computational details, we describe in detail both the basic features and the spirit of the method. Subsequently, the results concerning the VCD spectra of the previously cited selected systems are presented and discussed.

2 | Computational Details

2.1 | Details of the Molecular Dynamics Simulations and the Essential Dynamics Analysis

All the MD simulations were carried out using the Gromacs program, version 5.0.4 [75], following the standard common protocol described below. An initial energy minimization of the whole box was first carried out. The system was then gradually heated from 50 K to the temperature of interest (300 K, if

not otherwise stated) using short (200 ps) MD simulations. The simulation was propagated for the productive run (see Results section) in the NVT (constant number of molecules, volume, and temperature) ensemble using the Velocity rescaling algorithm for keeping the temperature constant [76]. The isobaric conditions in the NVT simulations were mimicked using a methodology recently proposed by our laboratory, based on adjusting the box size of the solute–solvent system to reproduce the average pressure previously obtained by simulating the same number of solvent molecules at the same temperature and at the liquid density corresponding to 1.0 bar. The LINCS algorithm was used to constrain all bond lengths [77]. Long-range electrostatics were computed by the Particle-Mesh Ewald method [78] using 34 wave vectors in each dimension and a 4th-order cubic interpolation. In all the simulations the CHARMM force field [79] and the SPC model [80] were used for the solutes and the solvent, respectively. Additional information, different for each of the investigated systems, is reported in the Results section. The ED analysis was performed as follows. At each frame of the simulation, the coordinates—or a subset of coordinates (see Results section)—of the species of interest were roto-translationally fitted to a reference structure to include only the "internal" degrees of freedom in the analysis. The corresponding covariance matrix was then constructed and diagonalized, providing a set of orthonormal eigenvectors and their corresponding eigenvalues—the former representing the eigendirections along which the fluctuation of the species of interest can be described, and the latter representing the extent of the fluctuations. The eigenvectors showing the largest eigenvalues, that is, the EEs, provide the subset of internal coordinates usable to follow the conformational transitions of the species of interest [22, 23]. In all the investigated systems, the convergence of the results was ascertained by repeating the ED-based conformation analysis on three sub-trajectories (portions) of the MD trajectories obtained from the rEMCS step. In all the cases, the results turned out to be virtually coincident. Additional details can be found in the Supporting Information (SI), Section S.5. Finally, a quantitative estimation of the agreement with experimental data was carried out by calculating the Root Mean Square Deviation (RMSD) of the experimental and calculated spectra as reported in detail in the SI (Section S.6). Note that this was accomplished by using the normalized intensities of both the experimental and the calculated spectra.

2.2 | Details of Quantum Chemical Calculations

The VCD spectra of all the extracted solute–solvent clusters were calculated in the framework of the Density Functional Theory (DFT) according to a common protocol described below. First, a constrained minimization was carried out for solute–solvent clusters extracted upon rEMCS. This was accomplished by freezing the following solute–solvent (internal) coordinates: (i) all the solute torsion angles (if any), (ii) the solvent molecules' center of mass in spherical coordinates defined with respect to the solute center of the mass, (iii) the torsion angles associated with the solvent rigid-body rotations with respect to the solute molecule and, finally, (iv) the solvent molecules' internal torsion angles (if any). The constrained-minimized structures $S(SOLV)_M$ were used for calculating the corresponding VCD spectra according to the standard procedures [36, 38] as implemented in the Gaussian16 software [81]. Each spectral line was then fitted to a Gaussian function with a bandwidth at $1/e$ peak height [82], the value of which is specified below for each system. The whole spectrum was finally obtained by summing the individual spectra of all the $S(SOLV)_M$ conformations, weighted for the corresponding probability ($p_{j,i}$) (see Results section). Additional information, different for each of the investigated systems, is reported in the Results section.

3 | Results

3.1 | Outline of the Method

In this preliminary section, we describe the sequence of all the steps, also pictorially represented in Figure 2, that make up the rEMCS computational strategy.

- *Step 1. MD-free simulation and solute conformational analysis.*

  The first step—common to all the cluster-in-solvent-based approaches—is aimed at determining the conformational space of the solute. This step, unnecessary if the solute is a rigid or semirigid molecule or if the solute conformational repertoire is well assessed (see below in the case of ADP), can be performed through an MD (or even MC) simulation of the whole system, hereafter termed *MD-free*, followed by standard methods of analysis such as the distribution of internal coordinates or ED (see S.I., Section S1 for details). As a result, a number of solute representative conformations with their statistical weights, p_i, are identified.

- *Step 2. MD-constrained simulation and the Ellipsoid-Method-for-Clusters-in-Solvent application.*

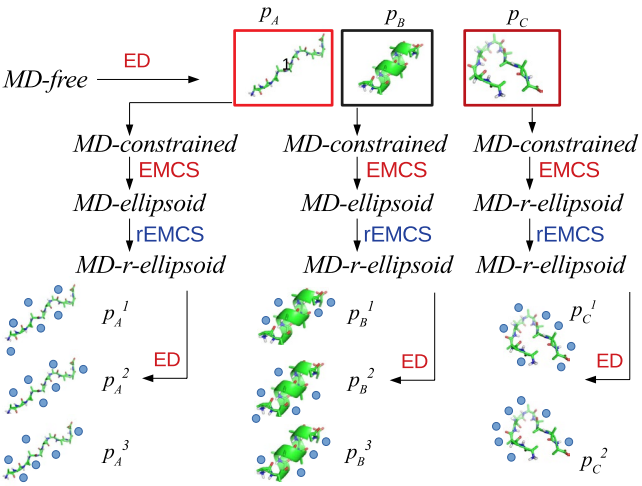

FIGURE 2 | Schematic summary of all the steps for collecting the ensemble of solute–solvent clusters from the rEMCS analysis. With p_i we indicate the probability of each solute conformational state as obtained from *MD – free*. With p_j^i we indicate the probability of each cluster conformational state as obtained from *MD-constrained*/EMCS/*MD-ellipsoid*/rEMCS/*MD-r-ellipsoid*/ED sequence. The water molecules are reported as blue spheres for the sake of clarity.

Each of the representative conformations extracted in the previous step is then independently simulated (see Figure 2) using the same box, number of solvent molecules, and protocol adopted for *MD-free*. In these new trajectories, termed as $MD-constrained$, the coordinates of the j-th representative conformation are kept frozen (restrained), with only the solvent molecules allowed to move, to reduce as much as possible the size of the conformational space, which must now necessarily include the solvation shells closer to the solute. For this purpose, from the application of EMCS to each of these $MD-constrained$, we obtain as many subtrajectories, hereafter termed as *MD-ellipsoid*, containing only the $S(SOLV)_M$ cluster with the frozen solute (S) and the M solvent (SOLV) molecules (see Figure 2). If the solute is not small enough [17], the number M of solvent molecules can become too large, and the corresponding ED analysis (see S.I. Section S1 for additional details) would suggest that an excessively large number of EEs would be necessary to analyze the solvent conformational space. The analysis thus becomes intractable, and in these cases, a simplification through rEMCS could be important.

- *Step 3. Ellipsoid reduction (rEMCS) and subsequent ED analysis*.

  Following the scheme depicted in Figure 2, at each frame of the *MD-ellipsoid*, using the same criterion followed for EMCS [17], we select a subset of solvent molecules conceivably defining the minimal solvation shell. The general strategy for this purpose, as already concisely represented in Figure 1, consists of selecting n solvent molecules interacting with each of the preselected l atoms of the solute, supposed—if any—to undergo tighter interactions with the solvent. Obviously, both n and l are arbitrary parameters that must be selected on the basis of the chemical features of the structure under study. The outcome of the rEMCS is, then, a new trajectory hereafter termed as *MD-r-ellipsoid*, containing the $k = n \times l$ solvent molecules and the solute. Note that the result is virtually coincident with what could be obtained by defining as many statistically correlated ellipsoids (and as many as the EMCS) as the selected l aggregation centers. The ED analysis, carried out on this *MD-r-ellipsoid*, would allow the extraction of the $S(SOLV)_k$ representative configurations, whose statistical weight p_i^j, should now take into account the statistical weight of the solute $i-th$ basin and the $S(SOLV)_k$ $j-th$ basin which are then used for calculating the spectral observable through Quantum Chemical calculations, as explained in the Computational Details Section and explicitly reported in the three following subsections.

3.2 | VCD Spectrum of Aqueous L-Alanine

The theoretical modeling of the VCD spectrum of aqueous L-Alanine (L-ALA) has been at the center of several studies, and it is now widely accepted that the explicit water distribution around the chiral solute significantly affects the VCD spectral features [83, 84]. Recently, Canuto and coworkers showed that, for a satisfactory agreement with the experimental spectrum, it is not only necessary to include, in the Quantum-Chemical calculations, the explicit water molecules of the first solvation shell, but it is also very important to take into account a huge number of solute–solvent-cluster structures, as obtained from MD simulations, mimicking what the authors call "thermal disorder" [12]. The sequential application of EMCS and rEMCS, followed by ED, as described in this section, reveals that the same level of accuracy can be reached by limiting the Quantum-Chemical calculations to a reduced number of *essential* microclusters, properly taking into account the water *first solvation shell*. The simulated system consisted of one L-ALA molecule inserted in a cubic box filled with 234 water molecules to sample the L-ALA conformational space. 100 ns of *MD-free* were produced and analyzed following the torsion angle (the only internal L-ALA coordinate excluding the conformationally irrelevant methyl and ammonium free rotations). The corresponding distribution, reported in Figure 3 clearly indicates that, as expected [12], in the simulated conditions, the complete rotation of the L-ALA torsion angle, however irrelevant for our purposes due to its 2-fold symmetry, occurs on time scales much larger than 100 ns.

For this reason, and according to the protocol described previously (Figure 2), we performed an $MD-constrained$ simulation, using the same conditions as the $MD-free$, keeping L-ALA frozen in the conformation corresponding to the maximum of the distribution reported in Figure 3. Application of EMCS on the $MD-constrained$ produced the $MD-ellipsoid$ subtrajectory of $L-ALA(H_2O)_{15}$ cluster (Figure 4a). The corresponding spectrum of the eigenvalues of the covariance atoms (black curve in Figure 4c) turned out to be not sufficiently steep to allow a relatively straightforward cluster analysis. Upon applying rEMCS by selecting four water molecules close to the carboxylate moiety and three close to the ammonium group, Figure 4b, produced the *MD-r-ellipsoid* subtrajectory of $L-ALA(H_2O)_{15}$ cluster. In this case, the spectrum of the eigenvalues of the covariance matrix (Figure 4c) allowed the use of only two EEs. The resulting 2D-free energy landscape (see Section S.1 and Equation S.1 in the S.I.) showed, indeed, four very sharp conformational basins (blue spots in the Inset (d) of Figure 4) corresponding to as many

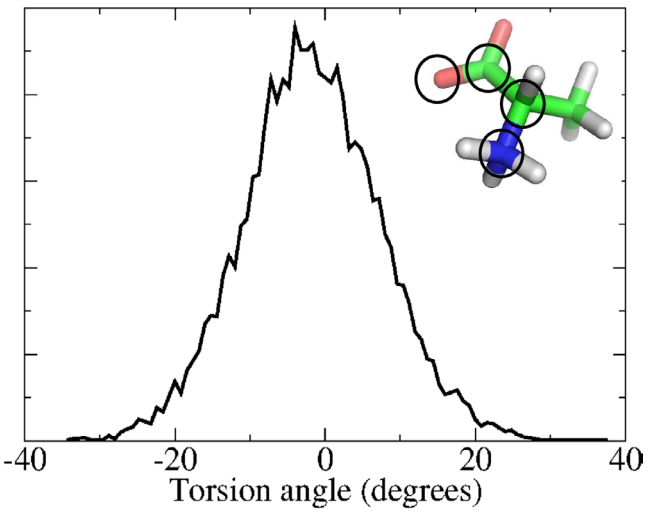

FIGURE 3 | Distribution of the L-ALA torsion angle (shown in the inset) sampled along the 100 ns of the $MD-free$ simulation.

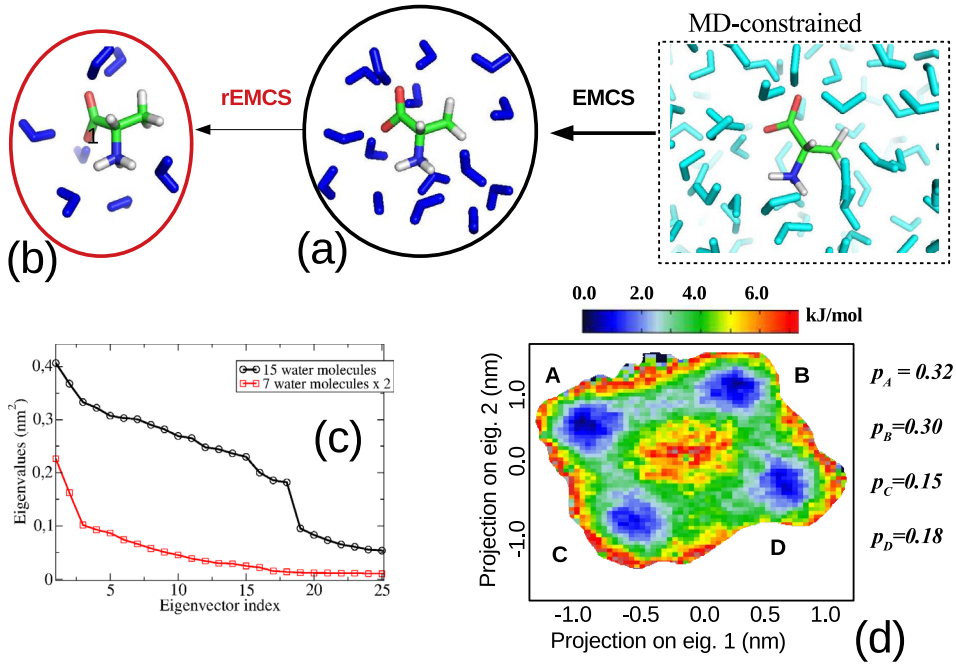

FIGURE 4 | (a) Snapshot of the $L-ALA(H_2O)_{15}$ cluster as obtained from the EMCS application to the *MD − constrained*. (b) Snapshot of the $L-ALA(H_2O)_7$ cluster as obtained from the application of the rEMCS to the *MD − ellipsoid*. (c) spectrum of the eigenvalues of the all-atom covariance matrix of $L-ALA(H_2O)_{15}$ (black curve) and $L-ALA(H_2O)_7$ (red curve) clusters. (d) 2D-free-energy landscape of the $L-ALA(H_2O)_7$ cluster. Note that in all these simulations, L-ALA was kept frozen.

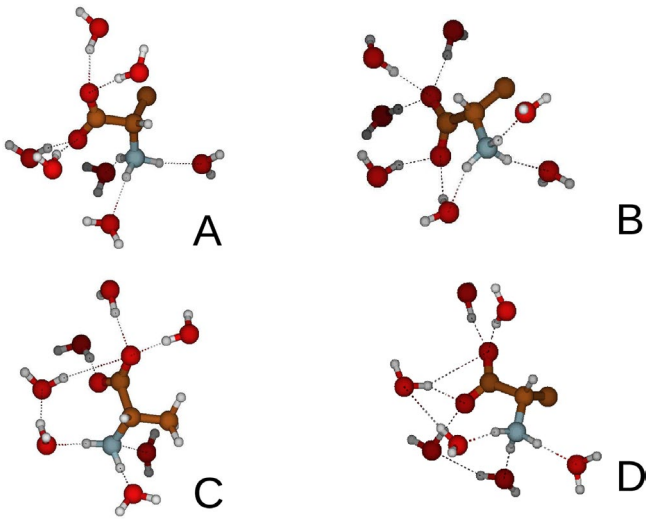

FIGURE 5 | Pictorial view of the representative conformations of the $L-ALA(H_2O)_7$ cluster of the four basins reported in Figure 4d.

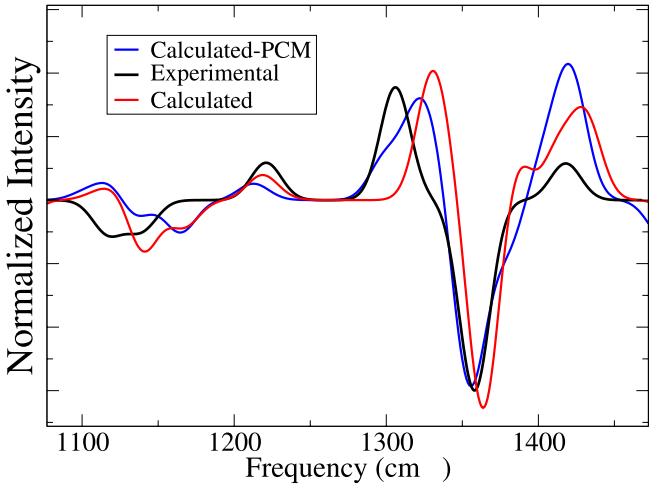

FIGURE 6 | Experimental (black) and calculated (red, and blue with PCM) VCD spectrum of L-ALA using the individual spectra of the representative conformations reported in Figure 5 and the corresponding probabilities reported in Figure 4d. A bandwidth of 7.0 cm^{-1} was used.

distinct representative conformations reported in Figure 5 and the coordinates of which are collected in the S.I. Section S2.

The spectra of each of these representative conformations, calculated as described in the Computational Details section using the B3LYP functional and the 6-311++G** basis set, were then weighted using the p_i reported in Figure 4d and, finally, summed. Additional details of the spectra are reported in the S.I. The final spectrum, depicted in Figure 6 in red, shows a deviation of 10.8 (RMSD, see SI, Section S.6) with respect to the experimental spectrum [85, 86]. The main discrepancies are essentially concentrated in the region between $1,300cm^{-1}$ and $1,400cm^{-1}$, where a significant blue shift of the two main peaks is observed, and also in the overestimation of the relative intensity of the peak at $1,418cm^{-1}$. For this reason, we decided to test the effect of the inclusion of mean-field by means of the Polarizable Continuum Model (PCM) [87]. The result, reported in the same figure in blue, shows a slight but significant shift to the blue, improving the result in the 1,300–$1,400cm^{-1}$ region. Nonetheless, other less positive effects, see for example the further increase of the signal beyond $1,400cm^{-1}$, should be remarked, and the whole RMSD (14.9) turned out to be slightly higher than that obtained without PCM. In conclusion, our

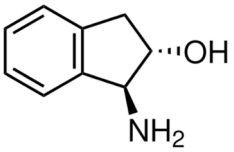

FIGURE 7 | Schematic view of (1S,2S)-trans-1-amino-2-indanol.

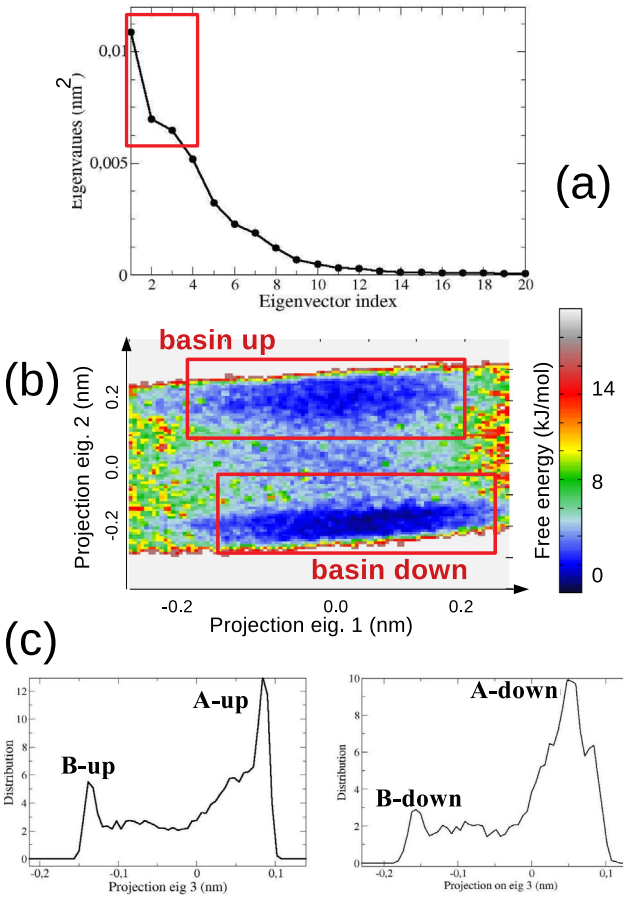

FIGURE 8 | (a) Spectrum of the eigenvalues from the diagonalization of the all-atom covariance matrix of trans-AI. The first eigenvector is characterized by concerted hydroxyl rotation and ring puckering; the second and third eigenvectors are characterized by in-phase and out-of-phase rotations of the amino and hydroxyl groups. (b) Free energy (Equation S.1 in the S.I.) landscape in the space of the first two eigenvectors of the all-atom covariance matrix. (c) Distribution of the projections on the third eigenvector of the all-atom covariance matrix of the trans-AI structures along the *MD – free*.

result is in good agreement with the findings of Canuto and coworkers, and confirms that, in the present case, the sequential application of EMCS-rEMCS-ED allows for properly capturing the essential features of the thermal disorder with a significantly reduced number (four) of DFT calculations.

3.3 | VCD Spectrum of (1S,2S)-Trans-1-Amino-2-Indanol in Dimethyl Sulfoxide

The second system examined in this study is (1S,2S)-trans-1-amino-2-indanol (trans-AI, see Figure 7) solvated in dimethyl sulfoxide (DMSO), whose VCD spectrum was recently reported by Zehnacker and coworkers [62]. They emphasized the crucial role of explicitly including DMSO molecules for accurate and reliable modeling. Trans-AI is characterized by three semiclassical large-amplitude internal degrees of freedom (i.e., alicyclic ring puckering, hydroxyl and amino group free-rotations) able, in principle, to produce a relatively high number of quasi-degenerate conformations [62]. For this reason, unlike the system presented in the previous paragraph—characterized by a single well-defined conformational internal coordinate—we employed ED for the preliminary conformational analysis of trans-AI. Following the protocol outlined in Figure 2, we first explored the conformational space of trans-AI using the *MD – free* simulation, which was propagated for 60.0 ns. This simulation was performed by placing a single trans-AI molecule in a cubic box filled with 180 DMSO molecules. The Gromos54a7 force field from the Automated Topology Builder [88] was used for both trans-AI and DMSO. Additional details can be found in the S.I. (Section S.3).

The spectrum of the eigenvalues (inset a of Figure 8) of the all-atom trans-AI covariance matrix, as obtained from ED analysis performed along the MD-free (see Section S.1 of the S.I.), clearly shows at least three EEs. Hence, to properly characterize the trans-AI conformational repertoire, we should use the first three eigenvectors (highlighted in red in the same figure), which account for more than 60 percent of the whole trans-AI internal fluctuations. For this purpose, at each frame of the *MD – free* we first projected the trans-AI coordinates onto the first two EEs obtaining the free-energy landscape (see Equation S.1 in the S.I.) depicted in the inset (b) of the Figure 8; the surface is characterized by two well separated conformational basins, indicated as *basinup* and *basindown*. Subsequently, all the structures falling in each of the two basins were then separately projected onto the third EE producing the bimodal distributions reported for the *basinup* and the *basindown* in the left and right side of the inset (c) of Figure 8, respectively. Four distinct trans-AI conformational states—corresponding to the maxima of the distributions, were then identified, namely *A – up* (probability 0.15), *B – up* (probability 0.25), *A – down* (probability 0.40), and *B – down* (0.20), and schematically reported in Figure 9.

These structures (see Figure 2) were used to run four independent *MD – constrained* simulations of 60.0 ns each, following the same protocol and simulation box as the *MD – free* simulation but keeping trans-AI frozen in its corresponding conformation, as reported in Figure 9. EMCS analysis of these simulations revealed that 15 DMSO molecules were necessary to properly define the ellipsoid that best approximates trans-AI. The ED analysis performed on the *MD – ellipsoid* simulations, as derived from EMCS, exhibited a very flat spectrum with extremely high eigenvalues, as shown in the upper part of panel (a) in Figure 10.

This characteristic, essentially due to the very high internal mobility of the DMSO molecules within the solvation shell formed by 15 molecules, made any type of cluster analysis impracticable, necessitating the adoption of rEMCS. Therefore, we decided to focus the analysis on only three DMSO molecules potentially capable of forming H-bonds with specific moieties of trans-AI, that is, the hydroxyl and the amino group. The ED analysis, carried out on the resulting *MD – r – ellipsoid* simulations, shows

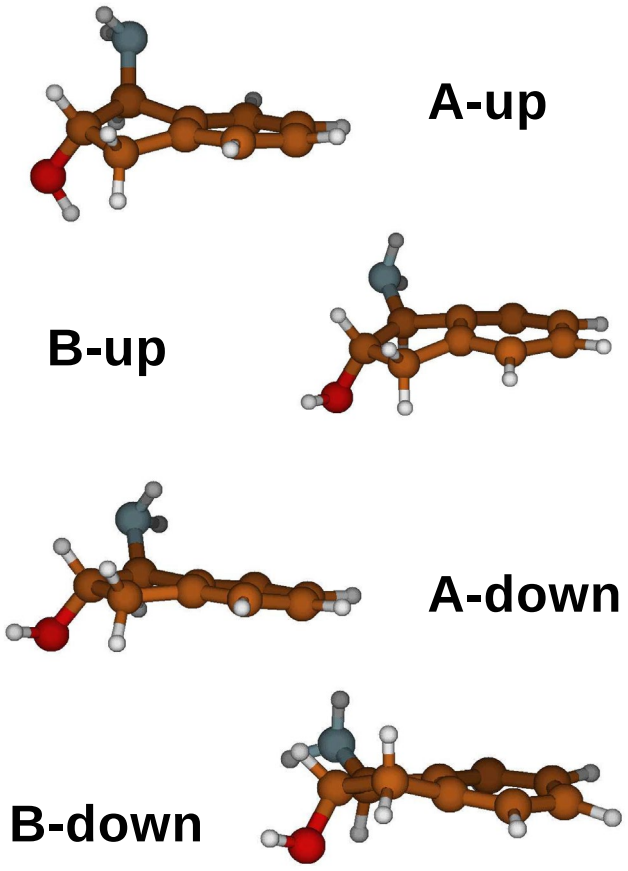

FIGURE 9 | Schematic view of the four structures of trans-AI extracted from the ED analysis outlined in the Figure 8.

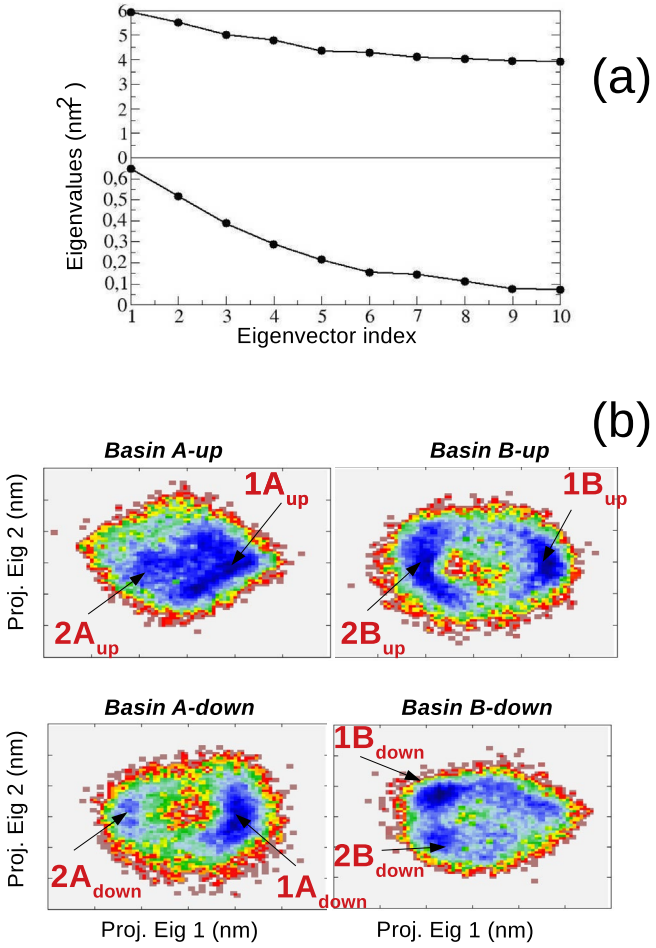

FIGURE 10 | (a) Spectrum of the eigenvalues for $trans-AI(dmso)_{15}$ (top panel) and $trans-AI(dmso)_3$ (bottom panel) ellipsoids. (b) Free energy landscapes (Equation S.1 in the S.I.) as obtained from the ED analysis on the four $MD-r-ellipsoid$ simulations.

a significant reduction in the conformational space (see panel (a) in Figure 9), which can be analyzed by considering only two EEs. By projecting on these EEs the $trans-AI(dmso)_3$ clusters sampled along the four $MD-r-ellipsoid$ trajectories, we obtained the free-energy conformational landscapes, reported in panel (b) of the same figure, from which it was possible to identify eight distinct $trans-AI-dmso_3$ clusters, indicated in Figure 11 along with their probabilities. These structures were finally utilized to calculate the VCD individual spectra, with details provided in the S.I.

The calculated VCD spectrum, reported in Figure 12, satisfactorily parallels the experimental one (RMSD equal to 8.0) with marked disagreements in correspondence of specific signals—either underestimated or overestimated—indicated by arrows. Neither the use of the PCM, as in the previous case, nor the use of a different basis set (data not shown) improved the result, for which a revision of the force field is perhaps necessary.

3.4 | Aqueous Di-Alanine Amide-III Band

The second example reported in this study is the VCD spectrum of aqueous capped di-Alanine (Ac-Ala-NHMe, ADP), with a particular focus on the Amide-III band, which has been specifically identified as a probe for detecting the conformational states adopted by ADP in water [74]. Also, for this system, the explicit inclusion of the water first solvation shell has been demonstrated to be essential for a correct modeling of spectral observables, either IR or VCD [9, 74]. Moreover, for a relatively flexible species like ADP, it is crucial to carefully consider the corresponding conformational repertoire of ADP and its related contribution to the actual spectral observables. In this respect, experimental [89] and theoretical studies [90] have well assessed that the population of aqueous ADP is dominated by polyproline *II* (P_{II}, about 60% of the whole population) followed by beta (β about 30% of the whole population) and right handed alpha (α_R) conformations. For this system, we then decided to skip the production of the $MD-free$ preliminary trajectory, instead using the well-established ADP conformational population and starting our study with the $MD-constrained$ independent simulations of the three constrained conformations. For all these simulations, we used one ADP molecule inserted into a cubic box filled with 5764 water molecules. The three simulations were extended up to 40.0 ns and independently analyzed to extract the solvation shell clusters. For this purpose, according to the general scheme previously outlined, we carried out the sequential EMCS and rEMCS procedures, which in this case allowed us to reduce the size of the solvation shell from 30 to 8 water molecules. We wish to remark that EMCS analysis carried out on the two

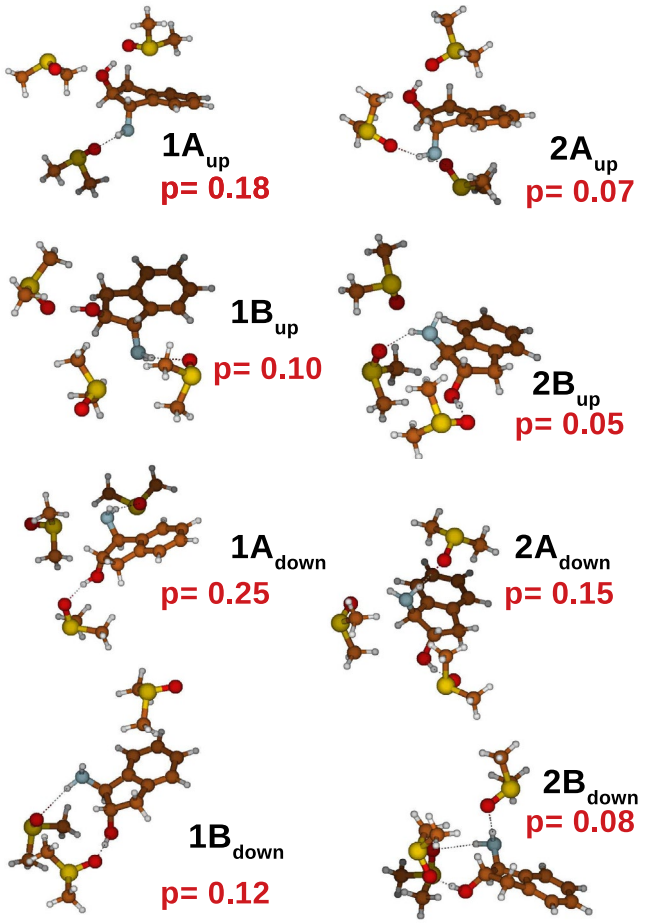

FIGURE 11 | Schematic view of the 8 structures of $trans-AI(dmso)_3$ extracted from the ED analysis (see Figure 10) and utilized for the calculation of the VCD spectrum. The corresponding probabilities are reported in red.

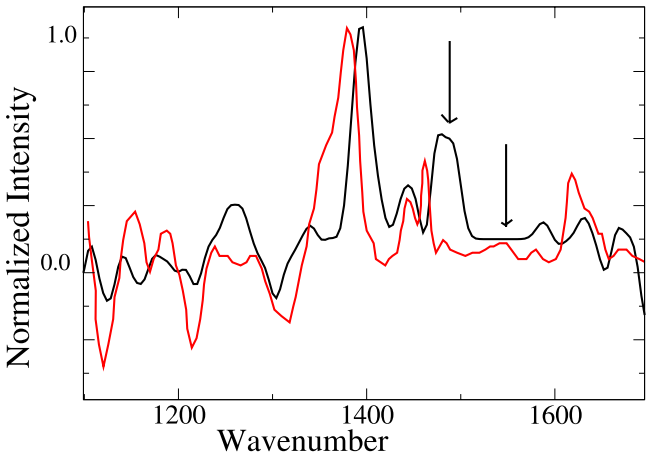

FIGURE 12 | Calculated (black) VCD spectrum using the structures of trans-AI, and corresponding probabilities reported in Figure 11, compared to the experimental one (red) [62].

halves of the *MD – constrained* simulations produced the same result, hence indicating the actual convergence of the solvent conformational sampling.

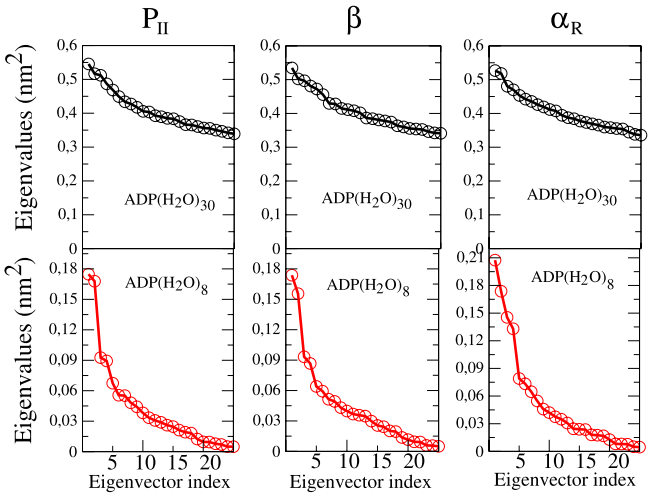

FIGURE 13 | Upper side: Spectra of the eigenvalues of the all-atom covariance matrix from ED analysis carried out onto the $ADP(H_2O)_{30}$ cluster trajectory as emerged from EMCS on the P_{II}, β and α_R *MD – constrained* simulations. Lower side: Spectra of the eigenvalues of the all-atom covariance matrix from ED analysis carried out onto the $ADP(H_2O)_8$ cluster trajectory as emerged from the rEMCS on the P_{II}, β and α_R *MD-ellipsoid* simulations from the previous step.

As shown in Figure 13, the passage from $ADP(H_2O)_{30}$ to $ADP(H_2O)_8$ drastically reduced the dimension of the (essential) conformational space allowing the use of the first two EEs for a proper representation of the $ADP(H_2O)_8$ conformational analysis. From the resulting free energy landscapes, reported in Figure 14, we could easily identify four (relatively) sharp free energy basins of the $ADP(H_2O)_8$ cluster for each of the ADP conformations. From these basins, we then extracted the corresponding representative conformations, one of which is reported in Figure 15, that is, corresponding to one of the P_{II}. Additional details, that is, the Cartesian coordinates and figures concerning all the other representative conformations, are reported in the S.I. Each of these representative conformations was finally used to model the corresponding VCD signals (see S.I. for details) at the B3LYP/6-31+G* level. The individual spectra, also reported in the S.I., were eventually merged using their weights (p_i, Figure 14) to obtain the signals for the three conformations shown in Figure 16. These signals successfully reproduce the characteristic band shape of the amide III region, that is, negative for the β conformation and positive for the other two conformations [74].

The whole spectrum in the amide III region, obtained by summing the signals reported in Figure 16 using the experimental relative population of P_{II}, β and α_R, is reported in Figure 17. Our result, closely similar to the spectrum obtained with a different computational approach [74], correctly reproduces the general experimental characteristics but significantly misses some of the fine structures observed in the red and blue regions. As a matter of fact, the calculated RMSD, order of magnitude higher than the previous cases (see SI, section S.6), testifies to the inability of our approach to reproduce the fine-structure characterizing (in particular) the red side of the experimental spectrum. In fact, if we restrict the RMSD to the central part of the spectrum (namely 1,260–1,350 cm^{-1}), we get a value of 9.6, in line with the corresponding values obtained for the other two systems. In any case, in the present study—specifically aimed at demonstrating

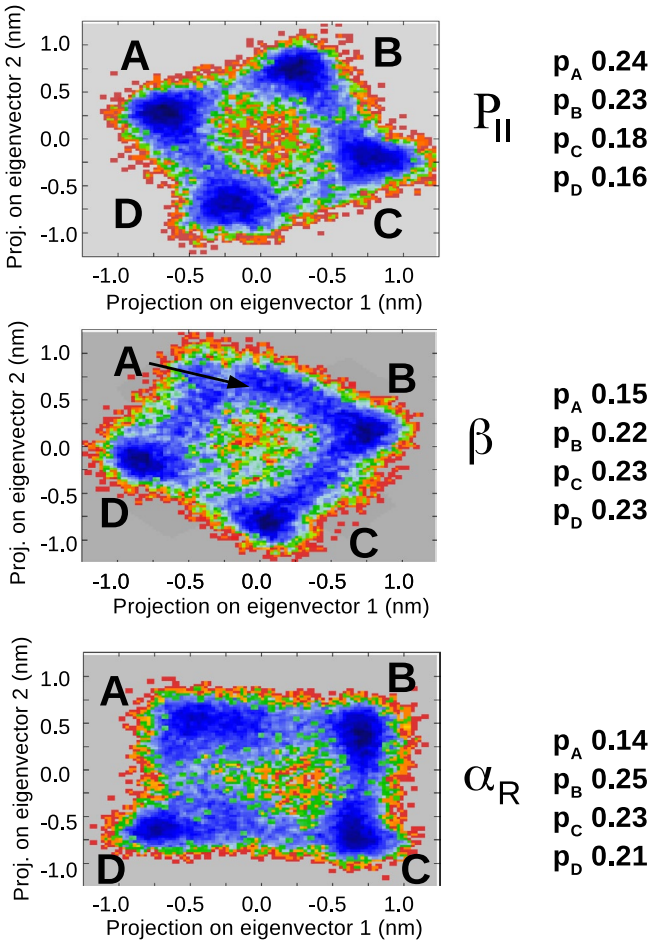

FIGURE 14 | Free energy landscape as a function of the projection of the $ADP(H_2O)_8$ coordinates onto the first two eigenvectors of the all-atom covariance matrix along the *MD-r-ellipsoid* of P_{II}, β and α_R. The statistical weights are also reported on the right side of the graphs.

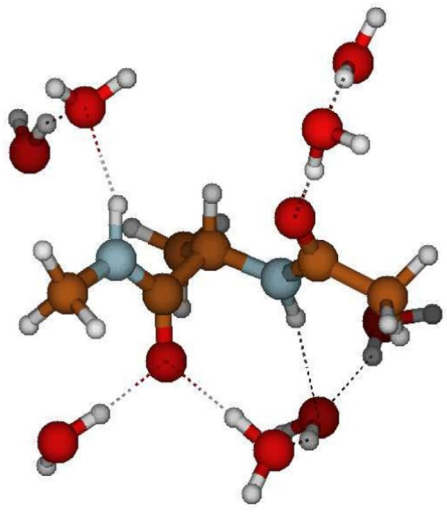

FIGURE 15 | Pictorial representation of the representative conformation for basin A from the ED analysis of the $ADP(H_2O)_8$ *MD-r-ellipsoid* analysis (see Figure 14).

the possibility of capturing the essential VCD features with a reduced number of conformations—we did not further investigate this aspect, although it is not irrelevant.

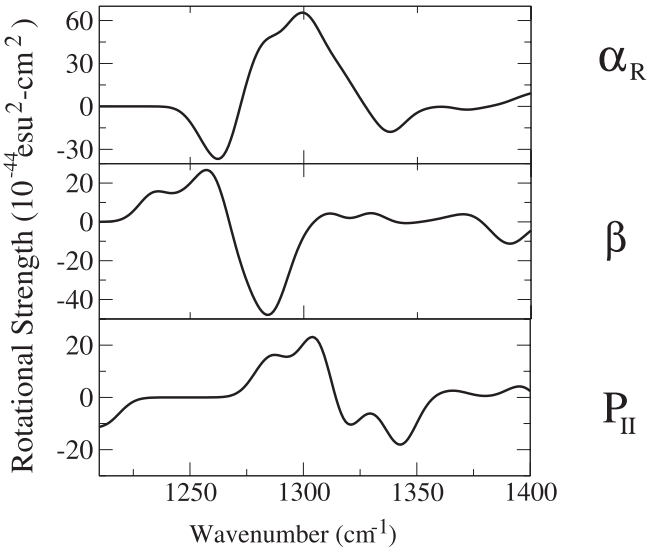

FIGURE 16 | Individual VCD spectra of ADP for P_{II}, β, and α_R as obtained by summing the spectra of the corresponding representative conformations VCD spectra using the statistical weights reported in Figure 14. A bandwidth of 7.0 cm^{-1} was used.

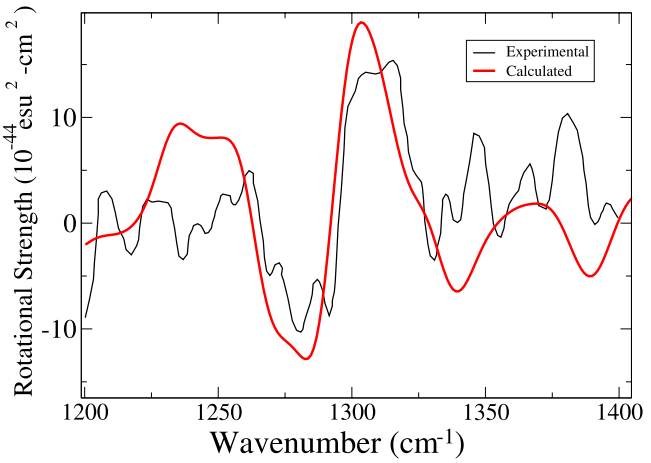

FIGURE 17 | Calculated (red) VCD spectrum of aqueous dialanine, superimposed with a reproduction [85] of the experimental one [86].

4 | Conclusions

One decade ago, our group proposed a computational protocol, based on the sequential application of the Ellipsoid-Method-for-Clusters-in-Solvent (EMCS) and Essential Dynamics (ED) methods for localizing solute–solvent microclusters as emerged from semiclassical MD simulations. The main, although not the unique, reason that prompted us to propose this method was the need for an unbiased protocol for identifying solute–solvent transient microclusters for the "Cluster-in-solvent" approach for computational spectroscopy. However, it was discovered that straightforward applications of the EMCS-ED were only possible for relatively small solutes in interaction with solvent molecules capable of undertaking strongly localized physical bonds (e.g., H-bonds). For this reason, we decided to propose a simple evolution of this protocol, termed as Reduced-EMCS (rEMCS), simply based on the elimination, from the cluster obtained by

EMSC, of a number of solvent molecules least interacting with the solute. The sequential application of the EMCS-rEMCS-ED on a series of semiclassical MD simulations was then presented in this study. The first reported example, the aqueous 10-ALA, has shown that even for relatively large solutes with peculiar shapes, rEMCS is able to identify a relatively sharp solute–solvent conformational repertoire. In the other two examples, aqueous L-alanine and aqueous capped di-alanine peptide, the validity of the method was also assessed by demonstrating that, with the use of a few number of solute–solvent microclusters, we could reproduce with satisfactory agreement the VCD spectral signals, known to be particularly sensitive to the solute–solvent interaction pattern. rEMCS could then be particularly suitable for highlighting other elusive features of the solvation shells, such as, for example, the chirality transfer currently under study in our laboratory.

Acknowledgments

We thank the European Union – NextGenerationEU under the Italian Ministry of University and Research (MUR) National Innovation Ecosystem grant ECS00000041—VITALITY—CUP E13C22001060006. We also thank the Italian Ministry of University for the PRIN-PNRR 2022 project "Organic Solar Cells: Identification and removal of charge recombination pathways"—CUP D53D2301724 0001. We also thank CINECA (Italy) for an ISCRA-C project and the use of computational resources. Open access publishing facilitated by Universita degli Studi dell'Aquila, as part of the Wiley - CRUI-CARE agreement.

Conflicts of Interest

The authors declare no conflicts of interest.

Data Availability Statement

The data that supports the findings of this study are available in the Supporting Information of this article.

References

1. V. Barone, S. Alessandrini, M. Biczysko, et al., "Computational Molecular Spectroscopy," *Nature Reviews Methods Primers* 1 (2021): 38.

2. A. Koleżyński, "Computational Methods in Spectroscopy," *Molecular Spectroscopy-Experiment and Theory* 26 (2019): 1–48.

3. T. L. Jansen, "Computational Spectroscopy of Complex Systems," *Journal of Chemical Physics* 155 (2021): 170901.

4. A. Segalina, J. Cerezo, G. Prampolini, F. Santoro, and M. Pastore, "Accounting for Vibronic Features Through a Mixed Quantum-Classical Scheme: Structure, Dynamics, and Absorption Spectra of a Perylene Diimide Dye in Solution," *Journal of Chemical Theory and Computation* 16 (2020): 7061–7077.

5. C. J. Cramer and D. G. Truhlar, "Implicit Solvation Models: Equilibria, Structure, Spectra, and Dynamics," *Chemical Reviews* 99 (1999): 2161.

6. C. G. Chen, M. Aschi, M. D'Abramo, and A. Amadei, "A Simplified Treatment for Efficiently Modeling the Spectral Signal of Vibronic Transitions: Application to Aqueous Indole," *Molecules* 27 (2022): 8135.

7. T. Giovannini, F. Egidi, and C. Cappelli, "Molecular Spectroscopy of Aqueous Solutions: A Theoretical Perspective," *Chemical Society Reviews* 49 (2020): 5664–5677.

8. G. Mancini, S. Del Galdo, B. Chandramouli, M. Pagliai, and V. Barone, "Computational Spectroscopy in Solution by Integration of Variational and Perturbative Approaches on Top of Clusterized Molecular Dynamics," *Journal of Chemical Theory and Computation* 16 (2020): 5747–5761.

9. K. Jalkanen, I. Degtyarenko, R. Nieminen, et al., "Role of Hydration in Determining the Structure and Vibrational Spectra of L-Alanine and N-Acetyl L-Alanine N′-Methylamide in Aqueous Solution: A Combined Theoretical and Experimental Approach," *Theoretical Chemistry Accounts* 119 (2008): 191.

10. Y. Kawashima, M. Dupuis, and K. Hirao, "Monte Carlo Microsolvation Simulations for Excited States Using a Mixed-Hamiltonian Model With Polarizable and Vibrating Waters: Applications to the Blueshift of the H2CO 1($\pi^*\leftarrow$n) Excitation," *Journal of Chemical Physics* 117 (2002): 248–257.

11. J. R. Pliego, Jr. and J. M. Riveros, "Hybrid Discrete-Continuum Solvation Methods," *Wiley Interdisciplinary Reviews: Computational Molecular Science* 10 (2020): e1440.

12. E. Orestes, C. Bistafa, R. Rivelino, and S. Canuto, "Including Thermal Disorder of Hydrogen Bonding to Describe the Vibrational Circular Dichroism Spectrum of Zwitterionic L-Alanine in Water," *Journal of Physical Chemistry. A* 119 (2015): 5099–5106.

13. B. Tirri, G. Mazzone, A. Ottochian, et al., "A Combined Monte Carlo/DFT Approach to Simulate UV-Vis Spectra of Molecules and Aggregates: Merocyanine Dyes as a Case Study," *Journal of Computational Chemistry* 42 (2021): 1054.

14. C. Sepali, S. Gómez, E. Grifoni, T. Giovannini, and C. Cappelli, "Computational Spectroscopy of Aqueous Solutions: The Underlying Role of Conformational Sampling," *Journal of Physical Chemistry. B* 128 (2024): 5083–5091.

15. H. C. Georg, K. Coutinho, and S. Canuto, "Solvent Effects on the UV-Visible Absorption Spectrum of Benzophenone in Water: A Combined Monte Carlo Quantum Mechanics Study Including Solute Polarization," *Journal of Chemical Physics* 126 (2007): 034507.

16. M. Steiner, T. Holzknecht, M. Schauperl, and M. Podewitz, "Quantum Chemical Microsolvation by Automated Water Placement," *Molecules* 26 (2021): 1793.

17. M. D'Alessando, A. Amadei, M. Stener, and M. Aschi, "Essential Dynamics for the Study of Microstructures in Liquids," *Journal of Computational Chemistry* 36 (2015): 399–407.

18. M. Monti, M. Stener, and M. Aschi, "A Computational Approach for Modeling Electronic Circular Dichroism of Solvated Chromophores," *Journal of Computational Chemistry* 2022 (2023): 43.

19. M. Monti, G. Brancolini, E. Coccia, et al., "The Conformational Dynamics of the Ligands Determines the Electronic Circular Dichroism of the Chiral Au38 (SC2H4Ph) 24 Cluster," *Journal of Physical Chemistry Letters* 14 (2023): 1941.

20. A. K. Jain, M. N. Murty, and P. J. Flynn, "Data Clustering: A Review," *ACM Computing Surveys* 31 (1999): 264.

21. R. Xu and D. Wunsch, "Survey of Clustering Algorithms," *IEEE Transactions on Neural Networks* 16 (2005): 645.

22. A. Amadei, A. B. Linssen, and H. J. Berendsen, "Essential Dynamics of Proteins," *Proteins* 17 (1993): 412.

23. I. Daidone and A. Amadei, "Essential Dynamics: Foundation and Applications," *Wiley Interdisciplinary Reviews: Computational Molecular Science* 2 (2012): 762–770.

24. P. Stephens and R. Clark, "Vibrational Circular Dichroism: The Experimental Viewpoint," in *Optical Activity and Chiral Discrimination: Proceedings of the NATO Advanced Study Institute Held at the University of Sussex, Falmer, England, September 10–22, 1978* (Springer, 1979), 263–287.

25. T. A. Keiderling, "Vibrational Circular Dichroism: Comparison of Techniques and Practical Considerations," in *Practical Fourier Transform Infrared Spectroscopy* (Elsevier, 1990), 203–284.

26. L. A. Nafie and R. K. Dukor, "Vibrational Circular Dichroism," in *Handbook of Vibrational Spectroscopy*, ed. J. M. Chalmers and P. R. Griffiths (John Wiley & Sons, 2002), 731–744.

27. P. L. Polavarapu and C. Zhao, "Vibrational Circular Dichroism: A New Spectroscopic Tool for Biomolecular Structural Determination," *Fresenius' Journal of Analytical Chemistry* 366 (2000): 727–734.

28. P. J. Stephens, F. J. Devlin, and J. R. Cheeseman, *VCD Spectroscopy for Organic Chemists* (CRC Press, Taylor and Francis, 2012).

29. G. Magyarfalvi, G. Tarczay, and E. Vass, "Vibrational Circular Dichroism," *Wiley Interdisciplinary Reviews: Computational Molecular Science* 1 (2011): 403–425.

30. H. Izumi, S. Yamagami, S. Futamura, L. A. Nafie, and R. K. Dukor, "Direct Observation of Odd- Even Effect for Chiral Alkyl Alcohols in Solution Using Vibrational Circular Dichroism Spectroscopy," *Journal of the American Chemical Society* 126 (2004): 194–198.

31. T. B. Freedman, X. Cao, R. K. Dukor, and L. A. Nafie, "Absolute Configuration Determination of Chiral Molecules in the Solution State Using Vibrational Circular Dichroism," *Chirality* 15 (2003): 743–758.

32. F. Zinna and G. Pescitelli, "Towards the Limits of Vibrational Circular Dichroism Spectroscopy: VCD Spectra of Some Alkyl Vinylethers," *Chirality* 28 (2016): 143–146.

33. T. A. Keiderling, "Structure of Condensed Phase Peptides: Insights From Vibrational Circular Dichroism and Raman Optical Activity Techniques," *Chemical Reviews* 120 (2020): 3381–3419.

34. E. Vass, M. Hollósi, F. Besson, and R. Buchet, "Vibrational Spectroscopic Detection of Beta-and Gamma-Turns in Synthetic and Natural Peptides and Proteins," *Chemical Reviews* 103 (2003): 1917.

35. V. Andrushchenko, H. Wieser, and P. Bouř, "B-Z Conformational Transition of DNA Monitored by Vibrational Circular Dichroism. Ab Initio Interpretation of the Experiment," *Journal of Physical Chemistry. B* 106 (2002): 12623.

36. L. Rosenfeld, "Quantenmechanische Theorie der natürlichen optischen Aktivität von Flüssigkeiten und Gasen," *Zeitschrift für Physik* 52 (1929): 161.

37. P. J. Stephens, "Theory of Vibrational Circular Dichroism," *Journal of Physical Chemistry* 89 (1985): 748–752.

38. J. Cheeseman, M. Frisch, F. Devlin, and P. Stephens, "Ab Initio Calculation of Atomic Axial Tensors and Vibrational Rotational Strengths Using Density Functional Theory," *Chemical Physics Letters* 252 (1996): 211.

39. P. L. Polavarapu, "Quantum Mechanical Predictions of Chiroptical Vibrational Properties," *International Journal of Quantum Chemistry* 106 (2006): 1809.

40. P. J. Stephens, F. J. Devlin, and J.-J. Pan, "The Determination of the Absolute Configurations of Chiral Molecules Using Vibrational Circular Dichroism (VCD) Spectroscopy," *Chirality* 20 (2008): 643–663.

41. J. R. Cheeseman, M. J. Frisch, and T. A. Keiderling, "Increased Accuracy of Vibrational Circular Dichroism Calculations for Isotopically Labeled Helical Peptides," *Spectrochimica Acta A* 313 (2024): 124097.

42. K. D. R. Eikås, M. T. Beerepoot, and K. Ruud, "A Computational Protocol for Vibrational Circular Dichroism Spectra of Cyclic Oligopeptides," *Journal of Physical Chemistry A* 126 (2022): 5458.

43. M. A. Koenis, L. Visscher, W. J. Buma, and V. P. Nicu, "Analysis of Vibrational Circular Dichroism Spectra of Peptides: A Generalized Coupled Oscillator Approach of a Small Peptide Model Using VCDtools," *Journal of Physical Chemistry. B* 124 (2020): 1665.

44. R. Gangemi, G. Longhi, and S. Abbate, "Calculated Absorption and Vibrational Circular Dichroism Spectra of Fundamental and Overtone Transitions for a Chiral HCCH Molecular Fragment in the Hypothesis of Coupled Dipoles," *Chirality* 17 (2005): 530–539.

45. F. Gangemi, R. Gangemi, G. Longhi, and S. Abbate, "Experimental and Ab-Initio Calculated Vcd Spectra of the First OH-Stretching Overtone of (1 R)-(–) and (1 S)-(+)-Endo-BORNEOL," *Physical Chemistry Chemical Physics* 11 (2009): 2683.

46. J. Bloino, "A VPT2 Route to Near-Infrared Spectroscopy: The Role of Mechanical and Electrical Anharmonicity," *Journal of Physical Chemistry. A* 119 (2015): 5269–5287.

47. T. R. Faulkner, C. Marcott, A. Moscowitz, and J. Overend, "Anharmonic Effects in Vibrational Circular Dichroism," *Journal of the American Chemical Society* 99 (1977): 8160–8168.

48. P. Polavarapu, "Vibrational Optical Activity of Anharmonic Oscillator," *Molecular Physics* 89 (1996): 1503.

49. M. Fusè, G. Longhi, G. Mazzeo, et al., "Anharmonic Aspects in Vibrational Circular Dichroism Spectra From 900 to 9000 Cm–1 for Methyloxirane and Methylthiirane," *Journal of Physical Chemistry. A* 126 (2022): 6719.

50. T. Kuppens, K. Vandyck, J. Van der Eycken, W. Herrebout, B. Van der Veken, and P. Bultinck, "Determination of the Absolute Configuration of Three As-Hydrindacene Compounds by Vibrational Circular Dichroism," *Journal of Organic Chemistry* 70 (2005): 9103.

51. P. L. Polavarapu and C. L. Covington, "Comparison of Experimental and Calculated Chiroptical Spectra for Chiral Molecular Structure Determination," *Chirality* 26 (2014): 539–552.

52. S. Góbi and G. Magyarfalvi, "Reliability of Computed Signs and Intensities for Vibrational Circular Dichroism Spectra," *Physical Chemistry Chemical Physics* 13 (2011): 16130–16133.

53. V. P. Nicu, E. Debie, W. Herrebout, B. Van der Veken, P. Bultinck, and E. J. Baerends, "A VCD Robust Mode Analysis of Induced Chirality: The Case of Pulegone in Chloroform," *Chirality* 21 (2009): E287.

54. J. Kubelka, R. Huang, and T. A. Keiderling, "Solvent Effects on IR and VCD Spectra of Helical Peptides: DFT-Based Static Spectral Simulations With Explicit Water," *Journal of Physical Chemistry. B* 109 (2005): 8231–8243.

55. Z. Dezhahang, C. Merten, M. R. Poopari, and Y. Xu, "Vibrational Circular Dichroism Spectroscopy of Two Chiral Binaphthyl Diphosphine Ligands and Their Palladium Complexes in Solution," *Dalton Transactions* 41 (2012): 10817–10824.

56. S. Góbi, E. Vass, G. Magyarfalvi, and G. Tarczay, "Effects of Strong and Weak Hydrogen Bond Formation on VCD Spectra: A Case Study of 2-Chloropropionic Acid," *Physical Chemistry Chemical Physics* 13 (2011): 13972–13984.

57. J. E. Rode, J. C. Dobrowolski, and J. Sadlej, "Prediction of l-Methionine VCD Spectra in the Gas Phase and Water Solution," *Journal of Physical Chemistry. B* 117 (2013): 14202–14214.

58. A. S. Perera, J. Thomas, M. R. Poopari, and Y. Xu, "The Clusters-In-a-Liquid Approach for Solvation: New Insights From the Conformer Specific Gas Phase Spectroscopy and Vibrational Optical Activity Spectroscopy," *Frontiers in Chemistry* 4, no. 9 (2016), https://www.frontiersin.org/journals/chemistry/articles/10.3389/fchem.2016.00009.

59. D. R. Galimberti, "Vibrational Circular Dichroism From DFT Molecular Dynamics: The AWV Method," *Journal of Chemical Theory and Computation* 18 (2022): 6217–6230.

60. T. Giovannini, G. Del Frate, P. Lafiosca, and C. Cappelli, "Effective Computational Route Towards Vibrational Optical Activity Spectra of Chiral Molecules in Aqueous Solution," *Physical Chemistry Chemical Physics* 20 (2018): 9181–9197.

61. B. Kirchner, J. Blasius, L. Esser, and W. Reckien, "Predicting Vibrational Spectroscopy for Flexible Molecules and Molecules With Non-Idle Environments," *Advanced Theory and Simulations* 4 (2021): 2000223.

62. K. Le Barbu-Debus, J. Bowles, S. Jähnigen, et al., "Assessing Cluster Models of Solvation for the Description of Vibrational Circular

Dichroism Spectra: Synergy Between Static and Dynamic Approaches," *Physical Chemistry Chemical Physics* 22 (2020): 26047–26068.

63. C. Merten, "Modelling Solute–Solvent Interactions in VCD Spectra Analysis With the Micro-Solvation Approach," *Physical Chemistry Chemical Physics* 25 (2023): 29404–29414.

64. J. R. Cheeseman, M. S. Shaik, P. L. Popelier, and E. W. Blanch, "Calculation of Raman Optical Activity Spectra of Methyl-*βi*-D-Glucose Incorporating a Full Molecular Dynamics Simulation of Hydration Effects," *Journal of the American Chemical Society* 133 (2011): 4991.

65. E. Debie, P. Bultinck, W. Herrebout, and B. van der Veken, "Solvent Effects on IR and VCD Spectra of Natural Products: An Experimental and Theoretical VCD Study of Pulegone," *Physical Chemistry Chemical Physics* 10 (2008): 3498–3508.

66. Z. Dezhahang, M. R. Poopari, and Y. Xu, "Vibrational Circular Dichroism Spectroscopy of Three Multidentate Nitrogen Donor Ligands: Conformational Flexibility and Solvent Effects," *Chemistry, an Asian Journal* 8 (2013): 1205–1212.

67. M. Losada, P. Nguyen, and Y. Xu, "Solvation of Propylene Oxide in Water: Vibrational Circular Dichroism, Optical Rotation, and Computer Simulation Studies," *Journal of Physical Chemistry. A* 112 (2008): 5621–5627.

68. S. Yang and M. Cho, "Direct Calculations of Vibrational Absorption and Circular Dichroism Spectra of Alanine Dipeptide Analog in Water: Quantum Mechanical/Molecular Mechanical Molecular Dynamics Simulations," *Journal of Chemical Physics* 131 (2009): 135102.

69. S. Jähnigen, D. Sebastiani, and R. Vuilleumier, "The Important Role of Non-Covalent Interactions for the Vibrational Circular Dichroism of Lactic Acid in Aqueous Solution," *Physical Chemistry Chemical Physics* 23 (2021): 17232–17241.

70. J. Bowles, S. Jähnigen, F. Agostini, et al., "Vibrational Circular Dichroism Spectroscopy With a Classical Polarizable Force Field: Alanine in the Gas and Condensed Phases," *ChemPhysChem* 25 (2024): e202300982.

71. S. Abbate, G. Longhi, K. Kwon, and A. Moscowitz, "The Use of Cross-Correlation Functions in the Analysis of Circular Dichroism Spectra," *Journal of Chemical Physics* 108 (1998): 50–62.

72. A. Scherrer, R. Vuilleumier, and D. Sebastiani, "Vibrational Circular Dichroism From Ab Initio Molecular Dynamics and Nuclear Velocity Perturbation Theory in the Liquid Phase," *Journal of Chemical Physics* 145 (2016): 084101.

73. M. Thomas and B. Kirchner, "Classical Magnetic Dipole Moments for the Simulation of Vibrational Circular Dichroism by Ab Initio Molecular Dynamics," *Journal of Physical Chemistry Letters* 7 (2016): 509–513.

74. A. Mirtič, F. Merzel, and J. Grdadolnik, "The Amide III Vibrational Circular Dichroism Band as a Probe to Detect Conformational Preferences of Alanine Dipeptide in Water," *Biopolymers* 101 (2014): 814–818.

75. M. Abraham, D. Van Der Spoel, E. Lindahl, and B. Hess, "GROMACS Development Teams at the Royal Institute of Technology and Uppsala University, Sweden," 2014.

76. G. Bussi, D. Donadio, and M. Parrinello, "Canonical Sampling Through Velocity Rescaling," *Journal of Chemical Physics* 126 (2007): 014101.

77. B. Hess, H. Bekker, H. J. Berendsen, and J. G. Fraaije, "LINCS: A Linear Constraint Solver for Molecular Simulations," *Journal of Computational Chemistry* 18 (1997): 1463.

78. T. Darden, D. York, and L. Pedersen, "Particle Mesh Ewald: An N Log (N) Method for Ewald Sums in Large Systems," *Journal of Chemical Physics* 98 (1993): 10089.

79. A. D. MacKerell, Jr., D. Bashford, M. Bellott, et al., "All-Atom Empirical Potential for Molecular Modeling and Dynamics Studies of Proteins," *Journal of Physical Chemistry. B* 102 (1998): 3586–3616.

80. H. J. Berendsen, J. P. Postma, W. F. van Gunsteren, and J. Hermans, "Interaction Models for Water in Relation to Protein Hydration," in *Intermolecular Forces: Proceedings of the Fourteenth Jerusalem Symposium on Quantum Chemistry and Biochemistry Held in Jerusalem, Israel, April 13–16, 1981* (Springer, 1981), 331–342.

81. M. J. Frisch, G. W. Trucks, H. B. Schlegel, et al., "Gaussian 16, Revision C.01," 2019.

82. P. J. Stephens and N. Harada, "ECD Cotton Effect Approximated by the Gaussian Curve and Other Methods," *Chirality* 22 (2010): 229–233.

83. K. Frimand, H. Bohr, K. J. Jalkanen, and S. Suhai, "Structures, Vibrational Absorption and Vibrational Circular Dichroism Spectra of L-Alanine in Aqueous Solution: A Density Functional Theory and RHF Study," *Chemical Physics* 255 (2000): 165–194.

84. M. D. Kundrat and J. Autschbach, "Modeling of the Chiroptical Response of Chiral Amino Acids in Solution Using Explicit Solvation and Molecular Dynamics," *Journal of Chemical Theory and Computation* 5 (2009): 1051–1060.

85. A. Rohatgi, "WebPlotDigitizer v. 5.2," (2022), https://automeris.io.

86. M. Diem, "Infrared Vibrational Circular Dichroism of Alanine in the Mid-Infrared Region: Isotopic Effects," *Journal of the American Chemical Society* 110 (1988): 6967–6970.

87. J. Tomasi and B. Mennucci, "Quantum Mechanical Continuum Solvation Models," *Chemical Reviews* 105 (2005): 2999.

88. A. Malde, L. Zuo, M. Breeze, et al., *Journal of Chemical Theory and Computation* 7 (2011): 4026.

89. J. Grdadolnik, V. Mohacek-Grosev, R. L. Baldwin, and F. Avbelj, "Populations of the Three Major Backbone Conformations in 19 Amino Acid Dipeptides," *Proceedings of the National Academy of Sciences* 108 (2011): 1794–1798.

90. N. G. Mirkin and S. Krimm, "Water Interaction Differences Determine the Relative Energetic Stability of the Polyproline II Conformation of the Alanine Dipeptide in Aqueous Environments," *Biopolymers* 97 (2012): 789–794.

Supporting Information

Additional supporting information can be found online in the Supporting Information section.